

DP-HLS: A High-Level Synthesis Framework for Accelerating Dynamic Programming Algorithms in Bioinformatics

Yingqi Cao*

University of California San Diego
San Diego, CA, USA

Jason Liang

University of California San Diego
San Diego, CA, USA

Anshu Gupta*

University of California San Diego
San Diego, CA, USA

Yatish Turakhia

University of California San Diego
San Diego, CA, USA

Abstract

Dynamic programming (DP) based algorithms are essential yet compute-intensive parts of numerous bioinformatics pipelines, which typically involve populating a 2-D scoring matrix based on a recursive formula, optionally followed by a traceback step to get the optimal alignment path. DP algorithms are used in a wide spectrum of bioinformatics tasks, including read assembly, homology search, gene annotation, basecalling, and phylogenetic inference. So far, specialized hardware like ASICs and FPGAs have provided massive speedup for these algorithms. However, these solutions usually represent a single design point in the DP algorithmic space and typically require months of manual effort to implement using low-level hardware description languages (HDLs). This paper introduces DP-HLS, a novel framework based on High-Level Synthesis (HLS) that simplifies and accelerates the development of a broad set of bioinformatically relevant DP algorithms in hardware. DP-HLS features an easy-to-use template with integrated HLS directives, enabling efficient hardware solutions without requiring hardware design knowledge. In our experience, DP-HLS significantly reduced the development time of new kernels (months to days) and produced designs with comparable resource utilization to open-source hand-coded HDL-based implementations and performance within 7.7–16.8% margin. DP-HLS is compatible with AWS[®] EC2 F1 FPGA instances. To demonstrate the versatility of the DP-HLS framework, we implemented 15 diverse DP kernels, achieving 1.3–32× improved throughput over state-of-the-art GPU and CPU baselines and providing the first open-source FPGA implementation for several of them. The DP-HLS codebase is available freely under the MIT license at <https://github.com/TurakhiaLab/DP-HLS> and its detailed wiki at <https://turakhia.ucsd.edu/DP-HLS/>.

1 Introduction

Genomic data is one of the fastest-growing data types globally, far outpacing Moore’s law in terms of data generation

[1]. To meet the rising computational demands of analyzing and interpreting this data, several efforts have focused on accelerating bioinformatics applications on hardware like GPUs, FPGAs, and ASICs [2–25].

While a lot of these accelerators are custom solutions to target a narrow application in bioinformatics, they also share notable similarities. For example, many of these solutions accelerate an algorithm based on dynamic programming (DP) [26]. This is unsurprising, as DP provides an efficient framework for comparing biological sequences—such as DNA, RNA, proteins, or even electrical signals from sequencing instruments—which is fundamental to many bioinformatics tasks, such as local pairwise alignments [27, 28], multiple sequence alignment [29, 30], homology searches [31, 32], whole-genome alignments [33], basecalling [34], and variant calling [35]. DP algorithms are computationally intensive, and therefore, they often dominate the runtime of these applications [36]. Recognizing their importance to bioinformatics, NVIDIA[®] recently introduced a specialized instruction, DPX, specifically to accelerate DP algorithms on GPUs [37].

Another key characteristic, particularly in FPGA and ASIC solutions [10–25], is the use of a hardware primitive—linear systolic arrays—that has been recognized since the 1980s for its efficiency in accelerating DP algorithms [38]. Most of these solutions focus on a specific or narrow set of 2-D DP algorithms and are typically designed at the Register Transfer Level (RTL) using low-level Hardware Description Languages (HDLs) like Verilog or VHDL, which makes them difficult to design and modify. A similar observation was made by a recent work, GenDP [39], which proposed a linear systolic array with software-programmable processing elements to accelerate a broad range of DP algorithms. However, software-programmable solutions introduce significant overhead on circuit-programmable FPGAs, which are the primary target of our work since they have already found commercial applications in bioinformatics [40–42].

In this paper, we present *DP-HLS*, a novel framework based on High-Level Synthesis (HLS) for accelerating broad DP kernels on FPGAs. A key feature of the framework is the

*Both authors contributed equally to this research.

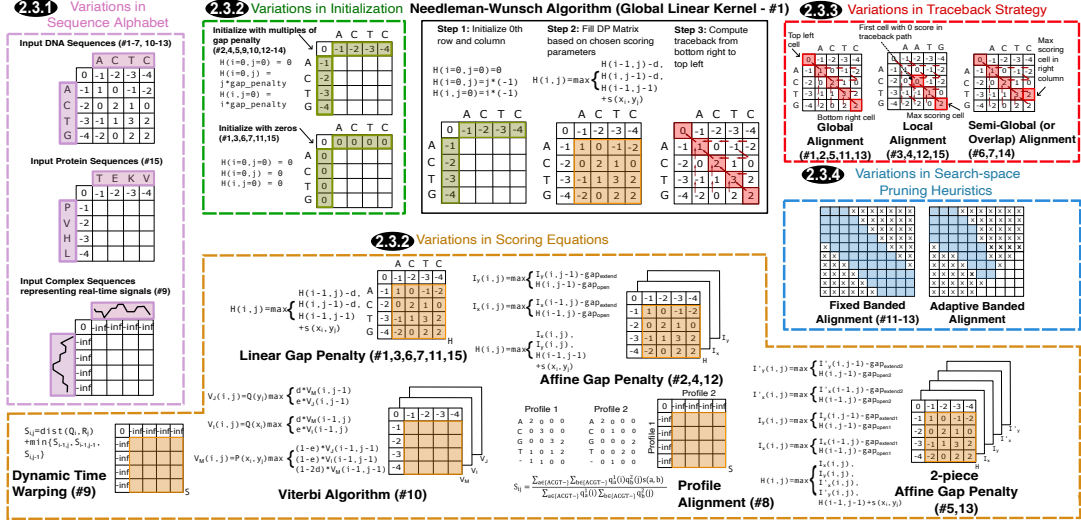


Fig. 1. Common variations in 2-D DP algorithms in Bioinformatics. Kernels are indexed using #'s based on Table 1.

separation of *back-end* optimizations from the *front-end* interface, enabling users to define new kernels in C++ without needing expertise in HLS or digital design. DP-HLS makes the following key contributions:

1. We developed DP-HLS, an HLS framework that, by separating front-end and back-end, introduces a layer of abstraction in the HLS flow to significantly enhance the productivity in deploying DP kernels on FPGAs. Specifically, the front-end provides a high degree of flexibility to specify new DP kernels in C++ without needing to add or modify HLS directives, while the back-end uses fixed HLS directives to efficiently translate these specifications into optimized RTL implementations with systolic arrays. Our experiments confirm that the generated RTL code exhibits the expected linear systolic array behavior.
2. Using the DP-HLS framework, we implemented 15 bioinformatically relevant DP kernels on FPGAs, covering a wide range of applications from basecalling to protein sequence alignment. All kernels are functionally verified and deployed on AWS[®] EC2 F1 instances for broad accessibility. For most kernels, no open-source FPGA implementations are available.
3. For the three DP kernels with available hand-optimized RTL implementations, DP-HLS achieved throughput within 7.7-16.8% and comparable resource utilization. However, DP-HLS significantly boosts design productivity, from months to days, compared to manual RTL design.
4. For several DP kernels implemented in state-of-the-art CPU and GPU libraries, DP-HLS delivered a 1.3–32× improvement in throughput over CPU- and GPU-optimized AWS[®] EC2 instances of the same cost.
5. We demonstrate, through an example, that recently proposed tiling heuristics [11] are compatible with DP-HLS

and can be used for performing both short and long sequence alignments on the FPGA.

6. We have made the entire framework publicly available, including all 15 DP kernels as case studies at <https://github.com/TurakhiaLab/DP-HLS>. Additionally, we provide a comprehensive wiki to assist new users at <https://turakhia.ucsd.edu/DP-HLS/>.

2 Background and Motivation

2.1 The 2-D Dynamic Programming Paradigm

Biological sequences, including DNA, RNA, and proteins, are the building blocks of life. DNA and RNA consist of four nucleotides: A, C, G, and T (U in RNA), while proteins are made up of 20 amino acids. Many bioinformatics problems involve comparing these biological sequences (DNA, RNA, proteins) to identify similarities and differences [60, 61]. A common approach is using 2-D dynamic programming (DP) algorithms (2-D DP paradigm), which typically include: i) *initialization*, ii) *matrix fill*, and iii) optional *traceback* [27, 62]. The *initialization* step arranges the two sequences on a 2-D grid, called *DP matrix*, with the first row and column having predefined scores. The *matrix fill* step uses a recursive formula to score each cell based on its three neighboring cells: above, left, and diagonal (Fig. 1). Lastly, the *traceback* step recovers the path in the DP matrix corresponding to the optimal score. Without traceback, only the optimal score is returned. Fig. 1 illustrates these steps using the most simplest 2-D DP algorithm, the Needleman-Wunsch algorithm [62].

2.2 Variations in the 2-D DP Paradigm

Table 1 shows a selection of 2-D DP kernels (indexed with '#' hereafter) that are commonly used in various bioinformatics applications, widely cited, and in some cases, targeted by

#	Alphabet	2-D DP Kernel	State-of-the-art Tools	Example Applications	Modifications in DP-HLS
1	DNA	Global Linear Alignment (Needleman-Wunsch)	BLAST[43], EMBOSS Stretcher[44]	Similarity Search	N/A
2	DNA	Global Affine Alignment (Gotoh)	BLAST[43], EMBOSS Needle[44]	Accurate Similarity Search	Scoring
3	DNA	Local Linear Alignment (Smith-Waterman)	BLAST[43], FASTA[45], BLAT[46]	Homology Search	Initialization and Traceback
4	DNA	Local Affine Alignment (Smith-Waterman-Gotoh)	BLAST[43], LASTZ[47]	Whole Genome Alignment	Scoring, Initialization and Traceback
5	DNA	Global Two-piece Affine Alignment	Minimap2[48]	Long Read Alignment	Scoring
6	DNA	Overlap Alignment	CANU[49], Flye[50]	Genome Assembly	Initialization and Traceback
7	DNA	Semi-global Alignment	BWA-MEM[51]	Short Read Alignment	Initialization and Traceback
8	Seq. Profiles	Profile Alignment	CLUSTALW[52], MUSCLE[30]	Multiple Sequence Alignment	Sequence Alphabet and Scoring
9	Complex Nos.	Dynamic Time Wrapping Algorithm (DTW)	SquiggleKit[53]	Basecalling	Sequence Alphabet and Scoring
10	DNA	Viterbi Algorithm (PairHMM)	HMMER[54], AUGUSTUS[55]	Remote Homology Search, Gene Prediction	Scoring (no Traceback)
11	DNA	Banded Global Linear Alignment	BLAST[43], Bowtie[56]	Fast Similarity Search	Scoring and Initialization
12	DNA	Banded Local Affine Alignment	Minimap2[48]	Long Read Assembly	Initialization, Scoring (no Traceback)
13	DNA	Banded Global Two-piece Affine Alignment	Minimap2[48]	Long Read Assembly	Scoring, Initialization and Traceback
14	Integers	Semi-global DTW (sDTW)	SquiggleFilter[57], RawHash[58]	Basecalling	Sequence Alphabet and Scoring
15	Amino acids	Local Linear Alignment with protein sequences	EMBOSS Water[44], BLASTp[43], DIAMOND[59]	Protein Sequence Alignment	Sequence Alphabet and Scoring

Table 1. Common bioinformatics kernels using 2-D DP algorithms, along with their associated tools, applications, and modifications relative to the baseline kernel (#1: Global Linear Alignment). Some tools implement multiple kernels.

hardware accelerators. We summarize key kernel characteristics and direct readers to original sources for details. These variations fall into four main categories (Fig. 1): i) *Sequence Alphabet*, ii) *Scoring Equations*, iii) *Traceback Strategy*, and iv) *Search-space Pruning Heuristics*, as outlined below.

2.2.1 Sequence Alphabet: An alphabet refers to the set of characters used to represent sequences, such as DNA, RNA, or protein, which typically consist of 4 or 20 characters, though some variations that introduce ambiguous bases, e.g., Ns, also exist [33, 43]. In Profile Alignment (#8), multiple DNA (protein) sequences are aligned with each other where each character is represented as a tuple of 5 (21) integers, referring to the frequencies of the 4 (20) nucleotides (amino acids) and gaps at each position of the alignment [63] (Fig. 1). Dynamic Time Warping (DTW) (#9 and #14), developed to compare two time-series signals [64, 65], uses real or complex numbers (Fig. 1) when used for basecalling in nanopore sequencing applications [57].

2.2.2 Scoring Equations: In the 2-D DP paradigm, scoring refers to the recurrence equations that calculate cell scores, by typically rewarding matches, and penalizing mismatches or gaps. We mention some of the scoring strategies and their common variations below.

(a) Substitution Scores: The simplest form of scoring uses a single value to reward a match or penalize a mismatch, or both. However, due to varying substitution frequencies (e.g., transitions vs. transversions), larger substitution matrices of penalty values are also common for DNA, RNA, or protein alignments [66] (Fig. 1). In Profile Alignments (#8) and DTW (#9), substitution values are computed dynamically using metrics like Sum-of-Pairs scoring [63] and Manhattan/Euclidean distance [57, 67], respectively.

(b) Gap Penalties: In sequence alignment, gap penalties penalize gaps (insertions or deletions). A linear gap penalty applies a constant penalty for every gap, while an affine gap penalty better models biological reality by assigning a higher penalty to opening a gap than extending an existing

gap [68]. This requires three score values (H, I, D) per DP-matrix’s cell. Minimap2 [48] uses a two-piece affine gap penalty with five values per cell to further improve the distinction between biological gaps and sequencing errors. In general, each affine layer adds two values to the DP matrix for gap cost to resemble a smooth convex function.

(c) Initialization: The scoring equations also define how the initial row and column are scored. Depending on which traceback strategy is used, the scores could be a constant (e.g., 0 or $-\infty$) or a function of the gap penalties (Fig. 1).

(d) Min/Max Objective Function: Most DP formulations (#1-7, #11-13) penalize the gap and find the maximum cell score, whereas DTW aims to find the minimum cell score while the score represents distances between the sequence. In this case, we need to replace the max function in recurrence equations with min (Fig. 1).

2.2.3 Traceback Strategy: The traceback step finds the actual alignment with the optimal score. While recurrence equations specify optimal transitions on a traceback path, the traceback strategy determines *where to start and end the path*. Four strategies are common: global, local, semi-global, and overlap, each influencing the recurrence and initialization equations (Fig. 1). *Global* strategy performs end-to-end whole genome sequence comparison, with a traceback path from the bottom-right to the top-left cell of the DP matrix. *Local* strategy finds similar subsequences and is used to identify conserved motifs or functional regions in sequences, with the traceback from the highest-scoring cell to a 0-scoring cell. *Semi-global* strategy matches one sequence end-to-end with a subsequence of the other, with the traceback starting from the bottom row’s highest-scoring cell to the top row. *Overlap* strategy, used in genome assembly, matches sequence ends (prefixes or suffixes) with traceback path from the highest-scoring cell in the rightmost column (bottom row) to the top row (leftmost column) of the 2-D DP matrix.

2.2.4 Search-space Pruning Heuristics: As 2-D DP matrices grow quadratically with sequence lengths, many algorithms employ heuristics like fixed or adaptive banding to prune unpromising regions (Fig. 1). *Fixed* banding algorithms compute cells near the main diagonal within a fixed distance [69], while *adaptive* methods like X-Drop [70] adjust band size dynamically based on cell scores.

3 An Overview of the DP-HLS Framework

DP-HLS is a framework that accelerates 2-D DP algorithms on FPGAs using HLS (Fig. 2). Built with AMD[®] Vitis HLS [71] tool, it offers customizability for creating FPGA-accelerated kernels tailored to specific applications. The framework consists of two components: the *front-end* (Section 4), where users can specify kernels in C/C++ without HLS expertise, supporting co-simulation, verification, and FPGA deployment; and the *back-end* (Section 5), which uses HLS directives to optimize the design for efficient hardware mapping. DP-HLS generalizes well across various 2-D DP kernels (e.g., to all kernels in Table 1), including the ones dealing with long sequence alignments.

4 Front-end Implementation

This section details the front-end of the DP-HLS framework, using examples from the 15 2-D DP kernels in Table 1 we implemented. Fig. 2A shows the design flow, involving kernel configuration, simulation, synthesis, co-simulation, and final implementation. The framework also provides debugging scripts and instructions for AWS[®] EC2 F1 FPGA deployment. Below, we outline the six required steps for configuring the front-end for specific kernels.

1 Customizing Data Types and Parameters: The DP-HLS framework supports custom data types of variable precision for scoring, traceback, and logic indices, enabling users to optimize efficiency for their specific kernel requirements. It also allows customization of scoring and input parameters. Primary front-end customizations are enumerated below.

1. Sequence Alphabets: As explained in Section 2.2.1, the sequence alphabet in 2-D DP kernels requires high configurability. DP-HLS addresses this by allowing users to define a custom data type, `char_t`, for the sequence alphabet. Listing 1 (left) shows a 2-bit unsigned integer used as `char_t` to represent the four nucleotide bases in DNA and RNA. Listing 1 (right) shows an alphabet for the DTW kernel (#9), where `char_t_st` is a struct of two 32-bit fixed-point numbers representing the real and imaginary parts of complex temporal signals being compared.

2. Scoring Layers and Data Types: As described in Section 2.2.2, some 2-D DP kernels involve multiple recurrence equations, each computing a unique value per cell. DP-HLS provides a variable, called `N_LAYERS`, in the front-end, which configures the number of unique values computed and stored per cell of the DP matrix. So, for kernels with an affine gap

penalty (Kernels #2, #4, #10, #12), `N_LAYERS` is set to 3, for those with a two-piece affine gap penalty (Kernels #5, #13), it is set to 5, and for the remaining kernels, it is set to 1.

3. Scoring Parameters: DP-HLS allows users to define an arbitrary number of scoring parameters with any data type in a C/C++ struct, called `ScoringParams`, with values set at runtime by the host code. Listing 2 (left) shows an example with three parameters (`match`, `mismatch`, and `linear_gap`) used by the Global Linear kernel (#1). The Viterbi kernel (#10) uses three states (M, I, and D) in the Hidden Markov Model and requires a total of 27 parameters. Two parameters, μ and λ , store the transition probabilities between the three hidden states, and a 5×5 emission matrix stores the emission probabilities for all pairs of characters (A, C, G, T, and $-$) in the M state (Listing 2 (right)).

4. Maximum Sequence Lengths: In DP-HLS, users can define maximum reference and query sequence lengths using `MAX_REFERENCE_LENGTH` and `MAX_QUERY_LENGTH`, which help determine the memory sizes for storing sequences and traceback pointers on the FPGA device. While the kernel supports fixed maximum lengths, longer sequences can be handled using software tiling approaches [12] using host-side code modifications.

5. Traceback Pointer Data Types and States: Traceback pointers in DP-HLS are stored in data type `tb_t` which users may define using arbitrary precision data type provided in Vitis HLS. For the Global Linear kernel (#1), `tb_t` is defined as `ap_uint<2>` and for the Global Affine kernel (#2), as `ap_uint<4>`, since the recurrence equations require a minimum of 2-bits and 4-bits, respectively, to represent the traceback pointers.

The traceback logic in the final step of DP algorithms is equivalent to a finite state machine (FSM) in which the current state and DP matrix cell score determine the next state and cell in the score matrix, which is translated to the traceback path. In DP-HLS, users enumerate the possible traceback states in the variable `TB_STATE`. For example, the Global Affine kernel (#2) enumerates three states — `MM`, `INS`, and `DEL` — representing match/mismatch, insertion, and deletion (Listing 3 (left)). In Listing 3 (right), the Global Two-piece Affine kernel (#5) has two extra traceback states (`LONG_INS`, `LONG_DEL`), one for each additional recurrence equation modeling long gap scores. The framework offers a no-`traceback` option, used by the Viterbi (#10) and Banded Local Affine (#12) kernels, to skip the traceback step.

6. Banding Width: DP-HLS allows users to use a fixed banding search space pruning strategy by setting the macros `BANDING` and `BANDWIDTH` to the desired band size.

2 Initializing Row and Column Scores: The DP-HLS framework includes two internal 2-D arrays, `init_row_scr` and `init_col_scr`, to store the scores of the initial row and column of the DP matrix, with the dimension of `MAX_REFERENCE_LENGTH` \times `N_LAYERS` and

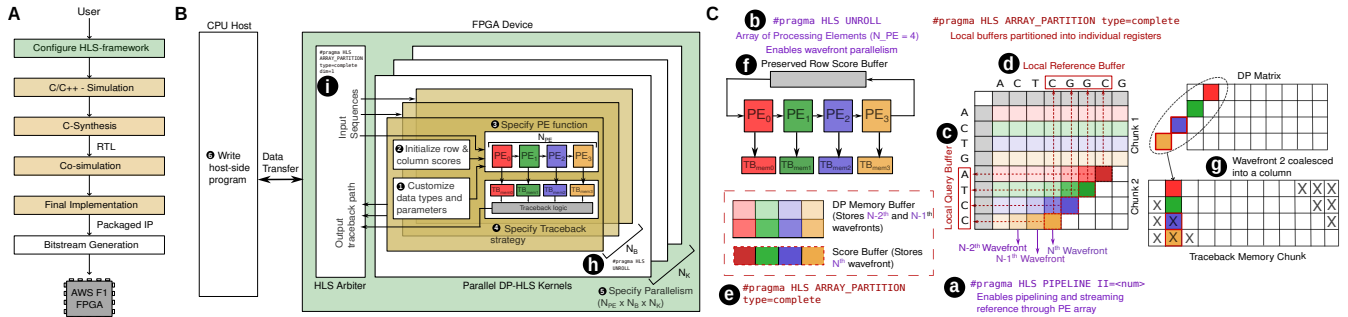


Fig. 2. DP-HLS implementation overview. (A) Basic workflow of DP-HLS kernels from user customization to FPGA deployment. (B) Front-end layout of DP-HLS kernels with customizable modules. (C) Key back-end optimizations with corresponding pragma directives.

```
typedef ap_uint<2> char_t;
struct char_t_st { ap_fixed <32, 26> real, imag; };
typedef char_t_st char_t;
```

Listing 1. Input alphabet for (Left) DNA sequences and (Right) complex number sequences.

```
struct ScoringParams {
  type_t mismatch;
  type_t match;
  type_t linear_gap;
} params;

struct ScoringParams {
  type_t log_mu;
  type_t log_lambda;
  type_t emission[5][5];
} params;
```

Listing 2. Definition of ScoringParams used in (Left) Global Linear kernel (#1) and (Right) Viterbi kernel (#10).

```
enum TB_STATE { MM, INS, DEL } tb_next_state, tb_curr_state;
enum TB_STATE { MM, INS, DEL, LONG_INS, LONG_DEL } tb_next_state, tb_curr_state;
```

Listing 3. Definition of traceback states for (Left) Global Affine (#2) and (Right) Global Two-piece Affine (#5) kernels.

```
type_t gap = scoring_params.linear_gap;
for (int i = 0; i < MAX_REFERENCE_LENGTH; i++){
  init_row_scr[i][0] = i*gap; }
for (int i = 0; i < MAX_QUERY_LENGTH; i++){
  init_col_scr[i][0] = i*gap; }
```

Listing 4. Initialization of column and row scores for Global Linear kernel (#1).

$MAX_QUERY_LENGTH \times N_LAYERS$, respectively. The users should specify the values of these arrays, as defining how DP-HLS would initialize them at the runtime. Listing 4 depicts the initialization step of the Global Linear kernel (#1), which has a single scoring layer at index 0 whose first row and column are initialized to account for gaps at the start of the alignment.

3 Specifying PE Function: In DP-HLS, all computations involved in the *matrix fill* step of the 2-D DP kernels (Section

```
type_t linear_gap = params.linear_gap;
type_t ins = dp_mem_left[0] + linear_gap;
type_t del = dp_mem_up[0] + linear_gap;
type_t match = dp_mem_diag[0] + (lc_qry_val == lc_ref_val) ? params.match : params.mismatch;
```

Listing 5. Definition of PE_func for Local Linear kernel (#3) computing the scores of the DP matrix.

```
type_t max_value = ins;
wt_tbp = TB_LEFT;
if (max_value < match){ max_value = match;
  wt_tbp = TB_DIAG; }
if (max_value < del){ max_value = del;
  wt_tbp = TB_UP; }
if (max_value < (type_t)0) { max_value = 0;
  wt_tbp = TB_END; }
wt_scr = max_value;
```

Listing 6. Logic for finding max cell score in the DP matrix and traceback pointer for Local Linear kernel (#3).

2.2.2) are executed by computing units known as *processing elements* (PEs). Within the DP-HLS front-end component, users only need to specify the recurrence equations for computing the score and traceback pointer for a single cell (i, j), located at row i and column j of the DP matrix. The back-end component automatically manages systolic communication between PEs and the storage of data in memory buffers. The recurrence equations are specified in PE_func (Listing 5) For example, in the Local Linear kernel (#3), the arrays dp_mem_up , dp_mem_diag , and dp_mem_left , are the inputs to PE_func and populated with cell scores by the DP-HLS back-end for cells at positions up ($i-1, j$), diagonal ($i-1, j-1$) and left ($i, j-1$) of the current cell (i, j). Likewise, the i^{th} query character and the j^{th} reference character are also automatically available to the input of PE_func as lc_qry_val and lc_ref_val , respectively. At the end of the function call, valid scores and traceback pointers for cell (i, j) must be stored to wt_scr and wt_tbp (Listing 6).

4 Specifying Traceback Strategy: An FSM intuitively defines the traceback logic in the final stage of the DP algorithm

```

if (tb_state == TB_STATE::MM){
  if (tb_ptr == TB_DIAG){tb_move = AL_MMI; }
  else if (tb_ptr == TB_UP){tb_move = AL_DEL; }
  else if (tb_ptr == TB_LEFT){tb_move = AL_INS; }
  else if (tb_ptr == TB_END) {tb_move = AL_END;}
  else {tb_move = AL_END;}
  tb_state = TB_STATE::MM;}

```

Listing 7. Definition of traceback logic state transitions for Local Linear kernel (#3).

(Section 2.2.3). Section 4.1.5 mentions the customization of the FSM states and traceback pointers. For multiple scoring matrices, each matrix maps to a state, and transitions represent jumps between matrices. Listing 7 defines the logic to map the current state and pointer to the next cell at each traceback step. In the Local Linear kernel (#3), a single state example, an outer if-statement checks the current `tb_state`, assigns the new state, and directs the traceback via `wt_tbp` for INS, DEL, MM, or AL_END (end of traceback).

5 Specifying Parallelism: The front-end component provides parameters (N_{PE} , N_B , N_K) that users can adjust to parallelize the synthesized design empirically, without understanding the internal details of the DP-HLS back-end and compiler optimizations. N_{PE} determines the level of *inner-loop parallelism* for a single pair of sequences. DP-HLS also exploits *outer-loop parallelism* across multiple sequence pairs by setting the parameters N_B and N_K . This allows the processing of $N_B \times N_K$ independent sequence pairs, with N_K independent channels to the host CPU (to take advantage of CPU multi-threading, for example), each consisting of N_B blocks sharing a single arbiter on the device, as shown in Fig. 2B. The design allows linking N_K heterogeneous kernels (e.g., a mix of global and local aligners) seamlessly in the design, a process that would be quite cumbersome with HDL.

6 Writing Host-Side Program: After completing the device specification, the user must define the host application to manage pre-processing and transfer of input sequences to the device, invoke device kernels, and receive alignment output from the device and/or perform tiling (for long reads). Effective scheduling is important to optimize device utilization; therefore, for optimal performance, it should be designed to schedule batches of input sequences and use multi-threading to leverage the device’s N_K independent channels. The host program uses OpenCL syntax [72], and relevant examples from our 15 implemented kernels (Table 1) are provided in the DP-HLS GitHub repository.

5 Back-end Implementation

The DP-HLS back-end component is based on the efficient mapping of 2-D DP algorithms to a linear systolic array, as extensively used in previous hardware accelerators [2, 10–21]. This enables various HLS optimizations to be encapsulated together without user modifications, thereby adding an abstraction layer to the HLS design, which helps boost

productivity. DP-HLS back-end also imposes design constraints on scoring and traceback stages to ensure optimal performance and configurability. Fig. 2B-C depicts the key back-end optimizations in DP-HLS using labels **a–i**. Optimizations **a–f** serve as hints to the HLS compiler to produce a linear systolic array of PEs that exploits *wavefront (anti-diagonal) parallelism* while computing the scores of the DP matrix, whereas optimizations **g–i** apply to the traceback logic and for exploiting inter-task parallelism. These optimizations are elaborated below.

5.1 Scoring Logic Design

Fig. 2C illustrates the scoring operation using an example of linear systolic array of four PEs ($N_{PE}=4$), which are used to compute the DP matrix. The rows of the DP matrix are divided into *chunks*, with each chunk containing N_{PE} consecutive rows, each assigned to a different PE (each row is color-coded according to the PE responsible for its computation). During the processing of a query chunk, each PE is initialized with the query base-pair corresponding to its row in the chunk while the reference sequence streams through the array. The systolic array architecture exploits the wavefront parallelism inherent in the computation of the query chunk. Chunk-wise score computation requires a buffer (Preserved Row Score Buffer) to store the scores computed by the last PE, which are then used by the first PE of next query chunk. The buffer size corresponds to the maximum length of the reference sequence in the DP matrix.

In the back-end component, the 2-D DP matrix is computed using the user-defined `PE_func` within nested for loops. The *outer loop* divides the matrix into chunks, the *middle loop* iterates through the wavefronts in this chunk, and the *inner loop* unrolls the PE function to map each score in the wavefront to its corresponding PE. Within the middle loop, the back-end applies optimization **a** using the `#pragma HLS PIPELINE` directive to enable wavefront pipelining. Each stage of the pipeline starts the computation of a new wavefront of the DP matrix using the unrolled PE array, while each PE in the array calls `PE_func` at the same cycle. The number of clock cycles between the initialization of each wavefront can be controlled by setting the *Initialization Interval (II)* of this directive, with $II=1$ as the optimum. For complex PE functions requiring more than 1 cycle per wavefront, HLS finds the minimum possible II to meet the timing requirement. At the inner loop, we apply optimization **b** using the `#pragma HLS UNROLL` directive to create a linear systolic array of PEs. However, to correctly and efficiently unroll the PEs, each input and output data element must be parallelly accessible for each PE. To ensure this, DP-HLS creates several fully partitioned local buffers that allow parallel data access using the `#pragma HLS ARRAY PARTITION variable=<buffer> type=complete` directive. For example, optimizations **c** and **d** apply this directive to create

local reference and query buffers, respectively, which store the sequence characters at the current wavefront. This directive is also used in the optimization **e** for DP Memory Buffer and Score Buffer, which stores the previous two wavefronts and the output scores of the current wavefront.

5.2 Traceback Logic and Memory Design

The optimal design of traceback logic and memory is essential for efficiency, as it typically consumes the most amount of memory resources in 2-D DP algorithms that require traceback. Below, we describe the two most critical optimizations implemented by the DP-HLS back-end component.

First, the back-end reorganizes the 2-D DP matrix so that the first dimension corresponds to N_{PE} , while the second dimension is scaled to accommodate the total pointers for user-specified maximum reference and query lengths, i.e., `MAX_REFERENCE_LENGTH` and `MAX_QUERY_LENGTH`, respectively. This reorganization ensures that each PE has access to a dedicated memory bank, allowing it to independently store its traceback (TB) pointers every cycle, thereby minimizing the II of the wavefront loop. The back-end further optimizes memory access by applying address coalescing, which translates consecutive wavefronts in the DP matrix to consecutive columns in the TB memory (see **g** in Fig. 2). This results in a more regular and efficient access pattern as all the PEs write their TB pointers to the same address in different memory banks. Additionally, the back-end automatically keeps track of the corresponding addresses each wavefront shall write in the TB memory.

Second, the back-end includes logic that allows users to configure the start and end conditions of the traceback. For instance, some traceback strategies require locating the maximum scores in the last row or column of the DP matrix. In such cases, each PE tracks its local maximum of the scores it computes if its coordinate satisfies the requirements (at the last row or column). Then, the DP-HLS back-end incorporates reduction logic to identify the maximum cell of the entire DP matrix block within a few cycles by a reduction maximum over each PE’s local max. The reduction operations happen once for each alignment block to determine the global maximum scoring cell.

5.3 Parallel Execution of Kernels

As described in Section 4, users specify parallelism using three parameters: N_K , N_B , and N_{PE} . The parallelism for N_{PE} is managed by the scoring logic optimizations discussed in Section 5.1, while N_K is handled by the linker. To enable parallel processing of N_B blocks within a kernel, DP-HLS uses two main optimizations. *First*, it uses `#pragma HLS UNROLL` to create multiple blocks within a kernel, allowing for the concurrent execution of these blocks (see **h** in Fig. 2). *Second*, it ensures concurrent memory access to the input and output buffers for each block through block-wise partition,

using `#pragma HLS ARRAY_PARTITION type=block dim=1`, with the number of partitions set to N_B (see **i** in Fig. 2).

6 Methodology

6.1 Datasets

DNA Sequences: The DNA sequences were generated using PBSIM2 [73] by simulating 1,000 PacBio [74] reads of 10,000 bases with a 30% error rate from the human reference genome GRCh38. For tiling version of Kernel #2, full reads were used. For short alignment kernels (#1-7, #10-13), each read was truncated to 256 bases.

Protein Sequences: Protein sequences for Kernel #15 were randomly sampled from UniProtKB (we used Swiss-Prot, 2024_03 release version, containing 571k entries) [75].

Complex Number Sequences: We simulated our own sequences using randomly generated complex numbers for input to the DTW kernel (#9).

sDTW Sequences: For the sDTW kernel (#14), we used the datasets used in the SquiggleFilter implementation [57].

Sequence Profiles: For the Profile Alignment kernel (#8), we generated profiles from randomly selected regions of 256 base pairs across the genomic sequences of *Drosophila melanogaster* and *Drosophila simulans*.

6.2 DP-HLS Framework Evaluation

Implementation: We implemented 15 DP-HLS kernels using C++(v17) (Table 1) and performed a C++-based simulation to verify the correctness of the final alignment output. The kernels are then synthesized using AMD[®] Vitis HLS 2021.2 tool [71], present on AWS[®] FPGA Developer AMI (v1.12.2), by following the complete design flow – from C/C++-Simulation to Bitstream Generation (Fig. 2A), and deployed on AWS[®] EC2 F1 instance (f1.2xlarge; with FPGA device XCVU9P-FLGB2104-2-1) using v++ command-line tools and OpenCL-based host code for host-kernel communication. For Kernel #2, we applied host-side code changes to support long alignments using a tiling heuristic [11]. A fixed target frequency of 250 MHz was set before synthesis. Parameters N_{PE} , N_B and N_K were configured for each kernel to maximize the device throughput (Table 2).

Throughput: Throughput for each DP-HLS kernel was calculated by using the number of clock cycles reported in the *co-simulation* step of AMD[®] Vitis HLS tool, maximum achievable frequency, and the number of parallel alignments computed on the FPGA device.

Resource Utilization: Post-routing reports of the bitstream generation step are used to obtain the Block RAMs (**BRAM**), Flip-Flops (**FF**), Lookup Tables (**LUT**), and Digital Signal Processors (**DSP**) utilization on the FPGA device for all kernels reported as a percentage of the total resources available on the AWS[®] EC2 F1 FPGA device.

Scalability: To examine the scalability of the kernels, we chose two diverse kernels, Global Linear (#1) and DTW (#9),

and evaluated their resource utilization and throughput values with increasing N_{PE} and N_B and fixed operating frequency of 250 and 200 MHz (Section 7.2).

6.3 Baseline Comparison

Software Baselines: We compared the throughput of DP-HLS Kernels #1-7, #11-12, #15 with state-of-the-art parallel CPU implementations, using SeqAn3 [76] (v3.3.0), a widely-used, multi-threaded bioinformatics library, as the baseline. For the Two-Piece affine (#5) and protein sequence alignment (#15) kernels, we used Minimap2 [48] (v2.28) and the command-line version of EMBOSS Water [44] (v6.6.0) as our software baselines, respectively. All software baselines were tested in a system with g++ (v10.3) and cmake (v3.16.3) and executed on a 36-core CPU-optimized AWS[®] EC2 instance, c4.8xlarge with 60 GB memory, which costs \$1.591 per hour, comparable to the AWS[®] EC2 F1 instance, f1.2xlarge (\$1.650 per hour) on which the DP-HLS throughput is estimated. The throughput values for SeqAn3 and Minimap2 were calculated by setting number of threads as 32 and considering the wall clock time of total execution. Since EMBOSS lacks multi-threading, we measured its throughput of 32 parallel jobs launched with GNU parallel. **Hardware Baselines:** We compared the FPGA throughput and resource utilization of the DP-HLS kernels with hand-crafted RTL implementations (*RTL Baselines*), GPU implementations (*GPU Baselines*), and previous HLS implementations (*HLS baselines*).

RTL Baselines: We obtained optimized open-source RTL implementations of GACT [11], Banded Smith-Waterman (BSW) [12] (v1) and SquiggleFilter [57] (v1.1.0) accelerators as RTL baselines to compare with Kernels #2, #12, and #14 (Table 1), respectively, since all are based on linear systolic array architecture, similar to DP-HLS kernels. The baselines are implemented using AMD[®] Vivado 2021.2 tool on the same AWS[®] EC2 F1 FPGA instance (f1.2xlarge), and resource utilization numbers were collected from the *Implementation* step. Throughput values for the first two were measured via Icarus Verilog simulations and BSW kernel via Vivado waveform simulations. To demonstrate the scaling effects, DP-HLS’s Kernel #2 was compared with GACT with increasing N_{PE} . The match-bonus feature in SquiggleFilter was removed to match Kernel #14’s implementation.

GPU Baselines: CUDASW++4.0 [77], which provides GPU implementation of the Smith-Waterman algorithm for protein sequences, was used as the baseline for DP-HLS Kernel #15. We disabled the traceback step in DP-HLS since it is not performed in the baseline. We used GASAL2 [5], with alignment type set as LOCAL, GLOBAL, BSW, as baselines for DP-HLS Kernels #4, #2, and #12, respectively. Both baselines were tested on an AWS[®] EC2 p3.2xlarge instance with NVIDIA[®] Tesla V100 GPU (costing \$3.06/hour). All throughput values were normalized for iso-cost comparison with the AWS[®] EC2 F1 FPGA instance (costing \$1.65/hour).

Kernel No.	Resource utilization for a 32PE block				Optimal (N_{PE} , N_B , N_K)	Max Freq (MHz)	Alignments/sec
	LUT	FF	BRAM	DSP			
#1	0.72%	0.42%	1.78%	0.029%	(64,16,4)	250.0	3.51×10^6
#2	1.30%	0.517%	1.78%	0.029%	(32,16,4)	250.0	2.85×10^6
#3	0.95%	0.63%	1.67%	0.014%	(32,16,5)	250.0	3.43×10^6
#4	1.60%	0.75%	1.67%	0.014%	(32,16,4)	250.0	2.71×10^6
#5	2.03%	0.65%	2.67%	0.029%	(32,8,5)	150.0	1.06×10^6
#6	0.98%	0.66%	1.67%	0.014%	(32,16,4)	250.0	2.73×10^6
#7	1.17%	0.67%	0.83%	0.014%	(32,16,4)	250.0	3.34×10^6
#8	3.66%	2.56%	2.56%	28.11%	(16,1,5)	166.7	3.70×10^4
#9	1.62%	1.55%	1.88%	2.84%	(64,4,3)	200.0	2.31×10^5
#10	3.78%	1.69%	1.67%	0.014%	(16,4,7)	125.0	4.90×10^5
#11	1.02%	0.40%	0.94%	0.029%	(64,8,7)	166.7	2.25×10^6
#12	1.44%	0.70%	0.57%	0.014%	(16,16,7)	200.0	4.77×10^6
#13	2.25%	0.69%	1.83%	0.029%	(16,8,7)	125.0	1.24×10^6
#14	1.22%	0.76%	0.57%	0.014%	(32,16,5)	250.0	5.16×10^6
#15	1.47%	0.95%	2.56%	0.014%	(32,8,5)	200.0	9.33×10^5

Table 2. Performance summary of 15 DP-HLS Kernels.

The kernel numbers correspond to the kernels listed in Table 1. Utilization in % of available FPGA resources is shown for a single block for 32 PEs for uniformity. We also show the optimal configuration of (N_{PE} , N_B , N_K) for each kernel that resulted in maximum throughput (alignments per second), and its corresponding maximum clock frequency and throughput achieved.

HLS Baselines: As HLS baselines, we used the AMD[®] Vitis Genomics Library, containing optimized Vitis HLS Libraries [78]. We used the 2021.2 branch, which works with the Vitis HLS 2021.2 version used for DP-HLS implementation. The Smith-Waterman kernel in this library matches with DP-HLS Kernel #3 implementation, so we chose it as our HLS baseline, with $N_{PE}=32$, $N_K=1$, $N_B=32$ and the maximum target clock frequency of 333 MHz.

7 Results

7.1 DP-HLS efficiently implements diverse 2-D DP kernels

Table 2 summarizes the performance and resource utilization of all 15 2-D DP kernels implemented on DP-HLS, as listed in Table 1. These kernels vary widely in terms of applications and computational patterns (Table 1), which is also evident from the range of hardware resource utilization and throughput values presented in Table 2.

For instance, when comparing the resource utilization of a single block of 32 PEs, Profile Alignment (#8) and DTW (#9) kernels have relatively higher DSP consumption. This is expected as these kernels perform multiplications, with Kernel #8 requiring two matrix-vector multiplications in each cell. For most other kernels, the DSP is only used for pre-computing traceback addresses.

The BRAM usage is primarily influenced by the complexity of traceback across most kernels. For instance, Kernels #5 and #13, which implement a two-piece affine gap penalty, require more BRAM as they need at least 7 bits to store each pointer, compared to only 2 bits per pointer for kernels with a linear penalty (e.g., Kernels #1 and #3). In Kernel #10 and

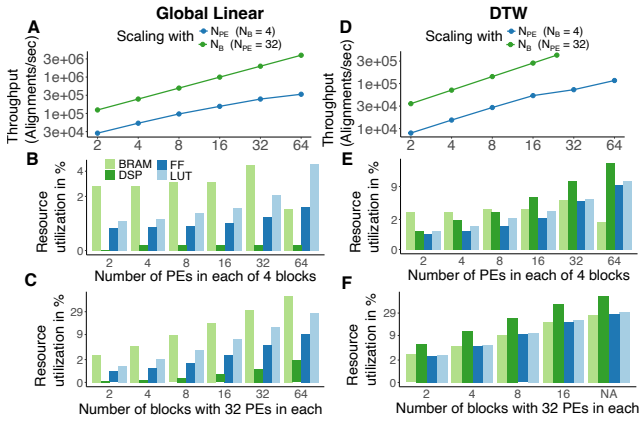


Fig. 3. Scaling results for Global Linear (#1) and DTW (#9) kernels with N_{PE} and N_B . (A, D) Throughput scaling of Global Linear (A) and DTW (D) in log-log scale with N_{PE} and N_B ; (B-C) Resource utilization scaling for Global Linear kernel; (E-F) Resource utilization scaling for DTW kernel.

#12, BRAM usage is minimal since traceback is not involved. Kernel #15, which deals with protein alignment, also consumes more BRAM to store the larger substitution matrix in ScoringParams (20×20 for protein sequences, compared to 4×4 for certain alignment algorithms of DNA sequences).

LUT and FF usage is mainly influenced by the complexity of the scoring equations. For instance, Kernel #8, with its complex matrix-vector multiplication, shows the highest FF and LUT utilization, followed closely by the Viterbi kernel (#10). Banding kernels (#11-13) also have slightly elevated logic usage due to the extra computations needed to determine the bands.

In terms of throughput, resource-intensive kernels (#8-10) have relatively lower values due to their complex computational patterns. For instance, Kernel #8 requires multiple cycles ($II=4$) to compute a single DP cell due to matrix-vector multiplications. The complexity of the scoring equations also impacts clock frequency, as seen in the Viterbi (#10) and Banded Global Two-piece Affine (#13) kernels. Overall, the resource utilization, clock frequency, and throughput numbers suggest that all kernels have been efficiently implemented by DP-HLS, which is also confirmed by the baseline comparisons presented later.

7.2 DP-HLS kernel implementations demonstrate 1-D systolic array behavior

Through the DP-HLS back-end optimizations, we would expect the HLS compiler to produce N_B 1-D systolic arrays, each with N_{PE} processing elements. However, since HLS-generated code is not easily interpretable, it is difficult to verify this directly from the code. Hence, we varied N_{PE} and N_B and checked if the throughput and resources scaled according to the expected behavior. Fig. 3 presents these results for two

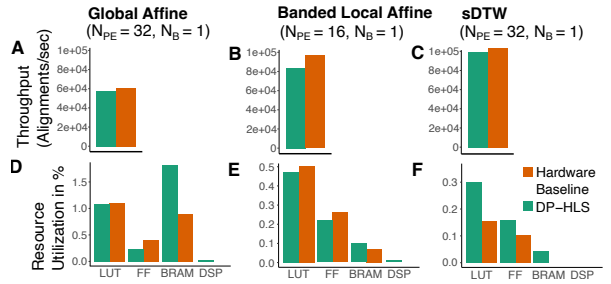


Fig. 4. Comparison of DP-HLS kernels (#2, #12, #14) with hardware baselines. (A-C) Throughput, and (D-F) Resource utilization comparison of Kernel #2 with GACT [11], Kernel #12 with BSW [12], Kernel #14 with Squiggle-Filter [57], respectively.

diverse kernels, Global Linear (#1) and DTW (#9), but we observed similar patterns across all 15 kernels.

Fig. 3A,D shows that throughput scales nearly perfectly with N_{PE} at lower values for both kernels but experiences some saturation at higher values. This is expected as the wavefront parallelism exploited by systolic arrays diminishes near the edges of the DP matrix, leading to more PEs with more idle cycles. In contrast, the large inter-alignment parallelism exploited by the N_B independent arrays allows throughput to scale almost perfectly with N_B , which is confirmed by the results for both kernels in Fig. 3. For DTW, N_B is capped at 24 as it reached maximum DSP availability.

Also, as we would expect, the percentage utilization of all resource types scales almost perfectly with increasing N_B while keeping N_{PE} constant (Fig. 3C, F). This occurs because each parallel block is identical, leading to a proportional increase in resource usage. When N_B is fixed, LUT and FF utilization scales perfectly with increasing N_{PE} for both kernels (Fig. 3B, E) due to the linear systolic array structure. However, DSP usage varies depending on the kernel's algorithm. For instance, DSP utilization scales well with increasing N_{PE} in the DTW kernel (Fig. 3E) as DSPs are used by each PE for the scoring logic, whereas for the Global Linear kernel, DSP usage remains constant (Fig. 3B) since DSPs are used for fixed logic outside the PEs to precompute the traceback starting address. Additionally, BRAM is primarily used for TB memory, which increases with N_{PE} up to 32 but does not scale proportionally. For higher N_{PE} values (e.g., $N_{PE}=64$), HLS compiler optimizations sometimes convert BRAMs to LUTRAMs to reduce memory access latency, resulting in lower BRAM usage.

7.3 DP-HLS kernels provide competitive performance to optimized RTL implementations

Fig. 4A-C compares the throughput of the three DP-HLS kernels: Global Affine (#2), Banded Local Affine (#12), and sDTW (#14), with the open-source RTL implementations of

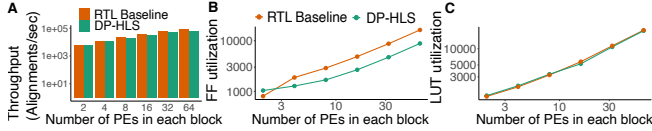


Fig. 5. Scaling comparison of DP-HLS kernels with hardware baselines (with increasing N_{PE} , $N_B=1$). (A) Throughput comparison (in log-log scale), and (B-C) FF and LUT scaling of Global Affine kernel (#2) with its hardware baseline, GACT, respectively.

domain experts, namely GACT [11], BSW [12] and Squiggle-Filter [57]. As mentioned in Section 6.3, we adjusted the N_{PE} and N_B values in DP-HLS to match those used in the baseline implementations. In all cases, we observed that DP-HLS achieves lower but competitive throughput to hand-crafted RTL implementations. Specifically, the DP-HLS throughput was within 7.7%, 16.8%, and 8.16% of the baseline for Global Affine, Banded Local Affine, and sDTW kernels, respectively. This is not surprising because, with added flexibility and programming ease, the DP-HLS framework misses out on some optimization opportunities that RTL implementations leverage. For example, all RTL implementations overlap query reads and DP matrix initialization with computation, but these steps are currently performed sequentially in DP-HLS. This overhead is even more apparent in the Banded Local Affine kernel, as it does not employ traceback. While we could perform a similar optimization in DP-HLS, we chose not to implement it, as the benefits are minimal, and it significantly complicates the front-end for end users. The relative throughput of the Global Affine kernel versus GACT remained consistent for long alignments, as both approaches use the same number of tiles.

The resource utilization comparison is more nuanced. For the Global Affine kernel, DP-HLS shows comparable LUT and FF usage compared to GACT (Fig. 4D). This is also reflected in the scaling behavior, where throughput remains similar (Fig. 5A), and the resource usage difference stays constant (Fig. 5B-C). DP-HLS also uses DSPs for pre-computing traceback starting addresses, unlike the baselines, but this does not affect scaling with N_{PE} . Despite this, DP-HLS has slightly better LUT and FF utilization on the Banded Local Affine kernel (Fig. 4E).

Overall, DP-HLS kernels demonstrate efficient resource scaling and competitive throughput compared to optimized RTL designs, with acceptable trade-offs for each kernel.

7.4 DP-HLS kernels provide 1.3× - 32× higher throughput than CPU and GPU baselines

We performed the iso-cost throughput comparison of DP-HLS with optimized open-source software libraries for applicable kernels on CPU and GPU instances on AWS[®] (Section 6.3). Fig. 6 summarizes these results. For Kernels #1-4, #6-7,

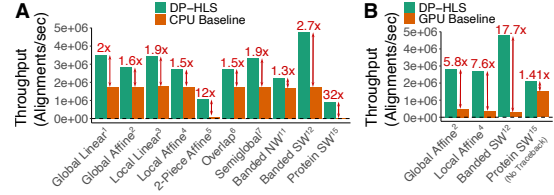


Fig. 6. Comparison of throughput values of various DP-HLS kernels with their (A) CPU and (B) GPU baselines. Kernels are referred from Table 1.

#11-12 (Table 1), the CPU baseline is SeqAn3, which DP-HLS outperforms by 1.5× to 2.7× (Fig. 6). Interestingly, the baseline throughput shows minor variability across these kernels as SeqAn3 uses the same underlying software implementation across kernels with minor adjustments. In contrast, DP-HLS applies various architectural optimizations tailored to each kernel, maximizing throughput by fitting multiple parallel kernels on the FPGA. For Kernels #5 and #15, which are computationally intensive, DP-HLS achieves higher relative throughput, 12×, and 32×, respectively (Fig. 6). This boost is likely due to DP-HLS’s use of arbitrary precision values and customized hardware data paths, enabling higher throughput than general CPU-based implementations.

Surprisingly, the relative performance of DP-HLS was better even when compared to GPU baselines—1.41× higher than CUDASW++ and 5.83-17.72× higher than GASAL2. Since GASAL2 codebase has not been updated recently, it might have been outpaced by newer CPU implementations, particularly in SeqAn3. To a lesser extent, DP-HLS also outperforms CUDASW++, which utilizes modern GPU optimizations, indicating that FPGAs may offer superior efficiency for DP algorithms. This observation is consistent with previous studies [79].

7.5 DP-HLS kernel outperforms a previous HLS baseline

We compared the HLS implementation of the Smith-Waterman algorithm provided in the AMD[®] Vitis Genomics Library (v2021.2) with Kernel #3 in DP-HLS. DP-HLS achieved 32.6% higher throughput than the HLS baseline. This difference could be explained by two factors. *First*, the HLS baseline uses streaming functions to transfer some data between the host and device for which the DP-HLS kernels use device memory. *Second*, DP-HLS backend adds more extensive optimization hints to the compiler than the baseline, which results in slightly higher resource utilization than the baseline but better throughput. We also note that it is significantly more challenging for new users to modify the HLS baseline to implement new 2-D DP kernels, as the HLS compiler directives (pragmas) are interleaved with the code that needs to be changed, resulting in a steeper learning curve compared to DP-HLS.

7.6 DP-HLS can improve the productivity of implementing new DP kernels by $\sim 10\times$

In addition to providing efficient FPGA implementations for 15 bioinformatically relevant DP kernels, most of which lack existing implementations, the DP-HLS framework aims to simplify the implementation and deployment of new DP kernels. Based on our experience, setting up the initial DP-HLS framework took several months, as we had to work through back-end optimizations and the quirks of HLS tools. This is similar to the timeline we have experienced for implementing such kernels in HDLs like SystemVerilog. Our experience suggests that current HLS does not necessarily offer a substantial productivity boost over RTL design. However, once the DP-HLS framework was in place, we were able to implement, test, and deploy new 2-D DP kernels on AWS[®] EC2 F1 instance in just 2–4 days. Hence, we think that HLS frameworks like DP-HLS, which separate high-level algorithmic specifications in the front-end from low-level optimizations in the back-end, for a broad algorithmic class, such as 2-D DP, can significantly enhance design productivity. For example, a similar framework could be developed for AI applications, mapping diverse matrix multiplication and convolution operations to 2-D systolic arrays [80–82].

8 Related Work

8.1 Dynamic Programming in Bioinformatics

Dynamic programming (DP) is an algorithmic paradigm that was first introduced in the 1950s by Bellman [26]. Needleman-Wunsch [62] is one of the earliest and best-known algorithms to have been applied to biological sequence comparison for global pairwise alignment. Since then, the 2-D DP paradigm has become immensely popular in bioinformatics, finding applications in local pairwise alignments [27, 28], multiple sequence alignment [29, 30], homology searches [31, 32], whole-genome alignments [33], basecalling [34], variant calling [35], and emerging applications like pangenomics [83, 84]. Given its computationally intensive nature and broad applicability, NVIDIA[®] recently introduced DPX instructions in Hopper GPUs to accelerate the DP paradigm [37]. DP-HLS also aims to modularize common 2-D DP algorithmic patterns in a flexible HLS framework, allowing users to easily customize kernels on FPGAs for various bioinformatics applications.

8.2 Systolic Array Accelerators for Bioinformatics Applications

Systolic arrays, introduced in the 1970s [85, 86], represent a major advancement in parallel computing by effectively distributing computational tasks across parallel units, with regular patterns of data movement between them. This architecture was initially applied for matrix multiplication [87], and by 1980s, it also found applications in bioinformatics using linear systolic arrays [38].

In recent years, many linear systolic array based FPGA and ASIC accelerators have been proposed for different bioinformatics applications [10–25]. Examples of such accelerators include GenASM, which accelerates the approximate string matching problem using the Bitap algorithm [24], SquiggleFilter, which accelerates a genomic surveillance application [57], and Darwin-WGA, which accelerates the X-Drop algorithm for whole-genome alignments [12]. Although these accelerators provide huge speedups for specific steps in genomic data analysis, they typically represent a single design point in the DP algorithmic space and cannot be easily refactored into other DP kernels due to their custom low-level HDL implementation. The goal of the DP-HLS framework is to boost design productivity in the development of 2-D DP kernels using HLS while providing competitive performance and similar resources to hand-crafted HDL implementations.

A recent work, GenDP [39], shares many similarities with the DP-HLS framework, as it also recognizes that many bioinformatics tasks rely on DP algorithms that are well-suited for systolic array implementations and provides a programmable framework to accelerate these tasks. However, GenDP’s programmability operates at the software level, where its processing elements have an instruction set that allows high-level DP algorithm specifications in the form of dataflow-graphs to be compiled. This makes GenDP a software-programmable ASIC. In contrast, DP-HLS targets dataflow architectures, such as FPGAs, where reprogramming involves reconfiguring the hardware itself. Unlike GenDP, DP-HLS kernels can be readily and efficiently deployed on cloud platforms with FPGA support, like AWS[®]. We also note that commercial bioinformatics accelerators, such as the DRAGEN[™] Bio-IT Processor by Illumina[®] [41], are based on FPGAs, where DP-HLS could be used for providing greater flexibility.

8.3 The Emergence of HLS Tools and Frameworks

High-Level Synthesis (HLS) allows users to design custom hardware using high-level languages, significantly reducing hardware development time. As a result, HLS tools and libraries have been widely adopted across various domains [88, 89], including machine learning [90, 91], cryptography [92, 93], and bioinformatics [94–97]. However, most previous works focus on implementing a single or a handful of kernels for specific applications, offering limited flexibility for users to configure new kernels. An exception in bioinformatics is the work of Benkrid et al. [97], who developed a flexible systolic array implementation of pairwise sequence alignment algorithms using Handel-C, a high-level HDL. This allowed users to customize hardware designs but only for a limited set of alignment algorithms (global, local, and overlap). While we could not directly compare to Benkrid et al. [97] as their codebase is not actively maintained, DP-HLS offers much greater flexibility within the 2-D DP paradigm,

allowing users to also configure scoring functions, scoring layers, input characters, traceback logic, and more.

9 Conclusion and Future Work

In this paper, we introduce DP-HLS, a novel HLS-based framework designed for FPGA acceleration of 2-D DP algorithms that are widely used in bioinformatics applications. DP-HLS allows users without hardware design experience to quickly develop efficient hardware solutions for DP algorithms with high flexibility. DP-HLS does this by introducing an abstraction layer in HLS design, which takes advantage of the fact that a broad range of applications can efficiently map to the same hardware primitive. DP-HLS is deployed on the AWS[®] cloud platform and achieves competitive throughput and similar resource utilization to hand-crafted RTL. In the future, we plan to implement HLS frameworks for other algorithmic classes, such as those used in AI and signal processing, using similar strategies.

10 Acknowledgments

We thank the AMD-omics group for helpful feedback. Research reported in this manuscript was supported by an Amazon Research Award (Fall 2022 CFP), AMD AI & HPC Fund, and the Hellman Fellowship.

References

- [1] Z. D. Stephens, S. Y. Lee, F. Faghri, R. H. Campbell, C. Zhai, M. J. Efron, R. Iyer, M. C. Schatz, S. Sinha, and G. E. Robinson, "Big data: astronomical or genomic?" *PLoS biology*, vol. 13, no. 7, p. e1002195, 2015.
- [2] J. Lindegger, D. Senol Cali, M. Alser, J. Gómez-Luna, N. M. Ghiasi, and O. Mutlu, "Scrooge: a fast and memory-frugal genomic sequence aligner for cpus, gpus, and asics," *Bioinformatics*, vol. 39, no. 5, p. btad151, 2023.
- [3] N. Ahmed, T. D. Qiu, K. Bertels, and Z. Al-Ars, "Gpu acceleration of darwin read overlapper for de novo assembly of long dna reads," *BMC bioinformatics*, vol. 21, pp. 1–17, 2020.
- [4] A. Zeni, G. Guidi, M. Ellis, N. Ding, M. D. Santambrogio, S. Hofmeyr, A. Buluç, L. Olikier, and K. Yelick, "Logan: High-performance gpu-based x-drop long-read alignment," in *2020 IEEE International Parallel and Distributed Processing Symposium (IPDPS)*. IEEE, 2020, pp. 462–471.
- [5] N. Ahmed, J. Lévy, S. Ren, H. Mushtaq, K. Bertels, and Z. Al-Ars, "Gasal2: a gpu accelerated sequence alignment library for high-throughput ngs data," *BMC bioinformatics*, vol. 20, pp. 1–20, 2019.
- [6] S. D. Goenka, Y. Turakhia, B. Paten, and M. Horowitz, "Segalign: A scalable gpu-based whole genome aligner," in *SC20: International Conference for High Performance Computing, Networking, Storage and Analysis*. IEEE, 2020, pp. 1–13.
- [7] S. Park, J. Hong, J. Song, H. Kim, Y. Kim, and J. Lee, "Agatha: Fast and efficient gpu acceleration of guided sequence alignment for long read mapping," in *Proceedings of the 29th ACM SIGPLAN Annual Symposium on Principles and Practice of Parallel Programming*, 2024, pp. 431–444.
- [8] Q. Aguado-Puig, S. Marco-Sola, J. C. Moure, C. Matzoros, D. Castells-Rufas, A. Espinosa, and M. Moreto, "Wfa-gpu: Gap-affine pairwise alignment using gpus," *bioRxiv*, pp. 2022–04, 2022.
- [9] A. Zeni, S. Onken, M. D. Santambrogio, and M. Samadi, "Leveraging difference recurrence relations for high-performance gpu genome alignment," in *Proceedings of the 2024 International Conference on Parallel Architectures and Compilation Techniques*, ser. PACT '24. New York, NY, USA: Association for Computing Machinery, 2024, p. 133–143. [Online]. Available: <https://doi.org/10.1145/3656019.3676894>
- [10] X. Fei, Z. Dan, L. Lina, M. Xin, and Z. Chunlei, "Fpgasw: accelerating large-scale smith–waterman sequence alignment application with backtracking on fpga linear systolic array," *Interdisciplinary Sciences: Computational Life Sciences*, vol. 10, pp. 176–188, 2018.
- [11] Y. Turakhia, G. Bejerano, and W. J. Dally, "Darwin: A genomics co-processor provides up to 15,000 x acceleration on long read assembly," *ACM SIGPLAN Notices*, vol. 53, no. 2, pp. 199–213, 2018.
- [12] Y. Turakhia, S. D. Goenka, G. Bejerano, and W. J. Dally, "Darwin-wga: A co-processor provides increased sensitivity in whole genome alignments with high speedup," in *2019 IEEE International Symposium on High Performance Computer Architecture (HPCA)*. IEEE, 2019, pp. 359–372.
- [13] A. Haghi, S. Marco-Sola, L. Alvarez, D. Diamantopoulos, C. Hagleitner, and M. Moreto, "An fpga accelerator of the wavefront algorithm for genomics pairwise alignment," in *2021 31st International Conference on Field-Programmable Logic and Applications (FPL)*. IEEE, 2021, pp. 151–159.
- [14] P. Zhang, G. Tan, and G. R. Gao, "Implementation of the smith-waterman algorithm on a reconfigurable supercomputing platform," in *Proceedings of the 1st international workshop on High-performance reconfigurable computing technology and applications: held in conjunction with SC07, 2007*, pp. 39–48.
- [15] R.-T. Chien, Y.-L. Liao, C.-A. Wang, Y.-C. Li, and Y.-C. Lu, "Three-dimensional dynamic programming accelerator for multiple sequence alignment," in *2018 IEEE Nordic Circuits and Systems Conference (NORCAS): NORCHIP and International Symposium of System-on-Chip (SoC)*, 2018, pp. 1–5.
- [16] P. Chen, C. Wang, X. Li, and X. Zhou, "Hardware acceleration for the banded smith-waterman algorithm with the cycled systolic array," in *2013 International Conference on Field-Programmable Technology (FPT)*, 2013, pp. 480–481.
- [17] D. Fujiki, S. Wu, N. Ozog, K. Goliya, D. Blaauw, S. Narayanasamy, and R. Das, "Seedex: A genome sequencing accelerator for optimal alignments in subminimal space," in *2020 53rd Annual IEEE/ACM International Symposium on Microarchitecture (MICRO)*, 2020, pp. 937–950.
- [18] J.-P. Wu, Y.-C. Lin, Y.-W. Wu, S.-W. Hsieh, C.-H. Tai, and Y.-C. Lu, "A memory-efficient accelerator for dna sequence alignment with two-piece affine gap tracebacks," in *2021 IEEE International Symposium on Circuits and Systems (ISCAS)*, 2021, pp. 1–4.
- [19] M.-J. Lin, Y.-C. Li, and Y.-C. Lu, "Hardware accelerator design for dynamic-programming-based protein sequence alignment with affine gap tracebacks," in *2019 IEEE Biomedical Circuits and Systems Conference (BioCAS)*, 2019, pp. 1–4.
- [20] E. J. Houtgast, V.-M. Sima, K. Bertels, and Z. Al-Ars, "An fpga-based systolic array to accelerate the bwa-mem genomic mapping algorithm," in *2015 International Conference on Embedded Computer Systems: Architectures, Modeling, and Simulation (SAMOS)*, 2015, pp. 221–227.
- [21] T. Oliver, B. Schmidt, D. Maskell, D. Nathan, and R. Clemens, "Multiple sequence alignment on an fpga," in *11th International Conference on Parallel and Distributed Systems (ICPADS'05)*, vol. 2, 2005, pp. 326–330.
- [22] S. Huang, G. J. Manikandan, A. Ramachandran, K. Rupnow, W.-m. W. Hwu, and D. Chen, "Hardware acceleration of the pair-hmm algorithm for dna variant calling," in *Proceedings of the 2017 ACM/SIGDA International Symposium on Field-Programmable Gate Arrays*, 2017, pp. 275–284.
- [23] S. Walia, C. Ye, A. Bera, D. Lodhavia, and Y. Turakhia, "Talco: Tiling genome sequence alignment using convergence of traceback pointers," in *2024 IEEE International Symposium on High-Performance Computer Architecture (HPCA)*. IEEE, 2024, pp. 91–107.
- [24] D. S. Cali, G. S. Kalsi, Z. Bingöl, C. Firtina, L. Subramanian, J. S. Kim, R. Ausavarungnirun, M. Alser, J. Gomez-Luna, A. Boroumand, A. Nori, A. Scibisz, S. Subramoney, C. Alkan, S. Ghose, and

- O. Mutlu, "GenASM: A High-Performance, Low-Power Approximate String Matching Acceleration Framework for Genome Sequence Analysis," Sep. 2020, arXiv:2009.07692 [cs, q-bio]. [Online]. Available: <http://arxiv.org/abs/2009.07692>
- [25] D. S. Cali, K. Kanellopoulos, J. Lindegger, Z. Bingöl, G. S. Kalsi, Z. Zuo, C. Firtina, M. B. Cavlak, J. Kim, N. M. Ghiasi *et al.*, "Segram: A universal hardware accelerator for genomic sequence-to-graph and sequence-to-sequence mapping," in *Proceedings of the 49th Annual International Symposium on Computer Architecture*, 2022, pp. 638–655.
- [26] R. Bellman, "Dynamic programming," *science*, vol. 153, no. 3731, pp. 34–37, 1966.
- [27] T. F. Smith, M. S. Waterman *et al.*, "Identification of common molecular subsequences," *Journal of molecular biology*, vol. 147, no. 1, pp. 195–197, 1981.
- [28] E. Ukkonen, "Finding approximate patterns in strings," *Journal of algorithms*, vol. 6, no. 1, pp. 132–137, 1985.
- [29] F. Sievers, A. Wilm, D. Dineen, T. J. Gibson, K. Karplus, W. Li, R. Lopez, H. McWilliam, M. Remmert, J. Söding *et al.*, "Fast, scalable generation of high-quality protein multiple sequence alignments using clustal omega," *Molecular systems biology*, vol. 7, no. 1, p. 539, 2011.
- [30] R. C. Edgar, "Muscle: a multiple sequence alignment method with reduced time and space complexity," *BMC bioinformatics*, vol. 5, pp. 1–19, 2004.
- [31] S. R. Eddy, "Profile hidden markov models." *Bioinformatics (Oxford, England)*, vol. 14, no. 9, pp. 755–763, 1998.
- [32] S. F. Altschul, W. Gish, W. Miller, E. W. Myers, and D. J. Lipman, "Basic local alignment search tool," *Journal of molecular biology*, vol. 215, no. 3, pp. 403–410, 1990.
- [33] R. S. Harris, *Improved pairwise alignment of genomic DNA*. The Pennsylvania State University, 2007.
- [34] J. T. Simpson, R. E. Workman, P. Zuzarte, M. David, L. Dursi, and W. Timp, "Detecting dna cytosine methylation using nanopore sequencing," *Nature methods*, vol. 14, no. 4, pp. 407–410, 2017.
- [35] R. Nielsen, T. Korneliusen, A. Albrechtsen, Y. Li, and J. Wang, "Snp calling, genotype calling, and sample allele frequency estimation from new-generation sequencing data," 2012.
- [36] A. Subramaniyan, Y. Gu, T. Dunn, S. Paul, M. Vasimuddin, S. Misra, D. Blaauw, S. Narayanasamy, and R. Das, "Genomicsbench: A benchmark suite for genomics," in *2021 IEEE International Symposium on Performance Analysis of Systems and Software (ISPASS)*. IEEE, 2021, pp. 1–12.
- [37] A. C. Elster and T. A. Haugdahl, "Nvidia hopper gpu and grace cpu highlights," *Computing in Science & Engineering*, vol. 24, no. 2, pp. 95–100, 2022.
- [38] R. J. Lipton and D. Lopresti, "A systolic array for rapid string comparison," in *Proceedings of the Chapel Hill conference on VLSI*. Chapel Hill NC, 1985, pp. 363–376.
- [39] Y. Gu, A. Subramaniyan, T. Dunn, A. Khadem, K.-Y. Chen, S. Paul, M. Vasimuddin, S. Misra, D. Blaauw, S. Narayanasamy *et al.*, "Gendp: A framework of dynamic programming acceleration for genome sequencing analysis," in *Proceedings of the 50th Annual International Symposium on Computer Architecture*, 2023, pp. 1–15.
- [40] S. Behera, S. Catreux, M. Rossi, S. Truong, Z. Huang, M. Ruehle, A. Visvanath, G. Parnaby, C. Roddey, V. Onuchic *et al.*, "Comprehensive genome analysis and variant detection at scale using dragen," *Nature Biotechnology*, pp. 1–15, 2024.
- [41] A. Goyal, H. J. Kwon, K. Lee, R. Garg, S. Y. Yun, Y. H. Kim, S. Lee, and M. S. Lee, "Ultra-fast next generation human genome sequencing data processing using dragentm bio-it processor for precision medicine," *Open Journal of Genetics*, vol. 7, no. 1, pp. 9–19, 2017.
- [42] TimeLogic® biocomputing solutions. [Online]. Available: <https://www.activemotif.com/catalog/75/timelogic-biocomputing-solutions>
- [43] NCBI, "Blast: Basic local alignment search tool," <https://blast.ncbi.nlm.nih.gov/Blast.cgi>, 2024, accessed: 2024-07-23.
- [44] F. Madeira, N. Madhusoodanan, J. Lee, A. Eusebi, A. Niewielska, A. R. N. Tivey, R. Lopez, and S. Butcher, "The embl-ebi job dispatcher sequence analysis tools framework in 2024," *Nucleic acids research*, p. gkae241, April 2024. [Online]. Available: <https://academic.oup.com/nar/advance-article-pdf/doi/10.1093/nar/gkae241/57199791/gkae241.pdf>
- [45] W. R. Pearson, "Using the fasta program to search protein and dna sequence databases," *Computer Analysis of Sequence Data: Part I*, pp. 307–331, 1994.
- [46] W. J. Kent, "Blat—the blast-like alignment tool," *Genome research*, vol. 12, no. 4, pp. 656–664, 2002.
- [47] R. S. Harris, *Improved pairwise alignment of genomic DNA*. The Pennsylvania State University, 2007.
- [48] H. Li, "Minimap2: Pairwise alignment for nucleotide sequences," *Bioinformatics*, vol. 34, no. 18, pp. 3094–3100, Sep. 2018, arXiv: 1708.01492 Publisher: Oxford University Press.
- [49] S. Koren, B. P. Walenz, K. Berlin, J. R. Miller, N. H. Bergman, and A. M. Phillippy, "Canu: scalable and accurate long-read assembly via adaptive k-mer weighting and repeat separation," *Genome research*, vol. 27, no. 5, pp. 722–736, 2017.
- [50] M. Kolmogorov, J. Yuan, Y. Lin, and P. A. Pevzner, "Assembly of long, error-prone reads using repeat graphs," *Nature biotechnology*, vol. 37, no. 5, pp. 540–546, 2019.
- [51] H. Li, "Aligning sequence reads, clone sequences and assembly contigs with bwa-mem," *arXiv preprint arXiv:1303.3997*, 2013.
- [52] J. D. Thompson, D. G. Higgins, and T. J. Gibson, "CLUSTAL W: Improving the sensitivity of progressive multiple sequence alignment through sequence weighting, position-specific gap penalties and weight matrix choice." *Nucleic Acids Research*, vol. 22, no. 22, pp. 4673–4680, Nov. 1994.
- [53] J. M. Ferguson and M. A. Smith, "SquiggleKit: a toolkit for manipulating nanopore signal data," *Bioinformatics*, vol. 35, no. 24, pp. 5372–5373, 07 2019. [Online]. Available: <https://doi.org/10.1093/bioinformatics/btz586>
- [54] R. D. Finn, J. Clements, and S. R. Eddy, "HMMER web server: Interactive sequence similarity searching," *Nucleic Acids Research*, vol. 39, no. Web Server issue, pp. W29–W37, Jul. 2011.
- [55] M. Stanke and B. Morgenstern, "Augustus: a web server for gene prediction in eukaryotes that allows user-defined constraints," *Nucleic acids research*, vol. 33, no. suppl_2, pp. W465–W467, 2005.
- [56] B. Langmead and S. L. Salzberg, "Fast gapped-read alignment with bowtie 2," *Nature methods*, vol. 9, no. 4, pp. 357–359, 2012.
- [57] T. Dunn, H. Sadasivan, J. Wadden, K. Goliya, K.-Y. Chen, D. Blaauw, R. Das, and S. Narayanasamy, "Squigglefilter: An accelerator for portable virus detection," in *MICRO-54: 54th Annual IEEE/ACM International Symposium on Microarchitecture*, 2021, pp. 535–549.
- [58] C. Firtina, N. Mansouri Ghiasi, J. Lindegger, G. Singh, M. B. Cavlak, H. Mao, and O. Mutlu, "Rawhash: enabling fast and accurate real-time analysis of raw nanopore signals for large genomes," *Bioinformatics*, vol. 39, no. Supplement_1, pp. 297–307, 06 2023. [Online]. Available: <https://doi.org/10.1093/bioinformatics/btad272>
- [59] B. Buchfink, K. Reuter, and H.-G. Drost, "Sensitive protein alignments at tree-of-life scale using diamond," *Nature methods*, vol. 18, no. 4, pp. 366–368, 2021.
- [60] S. K. Pal, S. Bandyopadhyay, and S. S. Ray, "Evolutionary computation in bioinformatics: A review," *IEEE Transactions on Systems, Man, and Cybernetics, Part C (Applications and Reviews)*, vol. 36, no. 5, pp. 601–615, 2006.
- [61] J. Cohen, "Bioinformatics—an introduction for computer scientists," *ACM Computing Surveys (CSUR)*, vol. 36, no. 2, pp. 122–158, 2004.
- [62] S. B. Needleman and C. D. Wunsch, "A general method applicable to the search for similarities in the amino acid sequence of two proteins," *Journal of molecular biology*, vol. 48, no. 3, pp. 443–453, 1970.
- [63] G. Wang and R. L. Dunbrack, "Scoring profile-to-profile sequence alignments," *Protein Science : A Publication of the Protein Society*, vol. 13,

- no. 6, pp. 1612–1626, Jun. 2004.
- [64] R. Bellman and R. Kalaba, “On adaptive control processes,” *IRE Transactions on Automatic Control*, vol. 4, no. 2, pp. 1–9, 1959.
- [65] R. Han, Y. Li, X. Gao, and S. Wang, “An accurate and rapid continuous wavelet dynamic time warping algorithm for end-to-end mapping in ultra-long nanopore sequencing,” *Bioinformatics*, vol. 34, no. 17, pp. i722–i731, 2018.
- [66] S. Henikoff and J. G. Henikoff, “Amino acid substitution matrices from protein blocks,” *Proceedings of the National Academy of Sciences of the United States of America*, vol. 89, no. 22, pp. 10 915–10 919, Nov. 1992. [Online]. Available: <https://www.ncbi.nlm.nih.gov/pmc/articles/PMC50453/>
- [67] H. Skutkova, M. Vitek, P. Babula, R. Kizek, and I. Provaznik, “Classification of genomic signals using dynamic time warping,” *BMC Bioinformatics*, vol. 14, no. S10, p. S1, Aug. 2013. [Online]. Available: <https://bmcbioinformatics.biomedcentral.com/articles/10.1186/1471-2105-14-S10-S1>
- [68] O. Gotoh, “An improved algorithm for matching biological sequences,” *Journal of Molecular Biology*, vol. 162, no. 3, pp. 705–708, Dec. 1982. [Online]. Available: <https://www.sciencedirect.com/science/article/pii/0022283682903989>
- [69] K.-M. Chao, W. R. Pearson, and W. Miller, “Aligning two sequences within a specified diagonal band,” *Bioinformatics*, vol. 8, no. 5, pp. 481–487, Oct. 1992.
- [70] Z. Zhang, S. Schwartz, L. Wagner, and W. Miller, “A Greedy Algorithm for Aligning DNA Sequences,” *Journal of Computational Biology*, vol. 7, no. 1–2, pp. 203–214, Feb. 2000.
- [71] “Vitis High-Level Synthesis User Guide,” 2021.
- [72] A. Munshi, B. Gaster, T. G. Mattson, and D. Ginsburg, *OpenCL programming guide*. Pearson Education, 2011.
- [73] Y. Ono, K. Asai, and M. Hamada, “PBSIM2: a simulator for long-read sequencers with a novel generative model of quality scores,” *Bioinformatics*, vol. 37, no. 5, pp. 589–595, Mar. 2021. [Online]. Available: <https://doi.org/10.1093/bioinformatics/btaa835>
- [74] A. Rhoads and K. F. Au, “PacBio Sequencing and Its Applications,” *Genomics, Proteomics & Bioinformatics*, vol. 13, no. 5, pp. 278–289, Oct. 2015.
- [75] The UniProt Consortium, A. Bateman, M.-J. Martin, S. Orchard, M. Magrane, S. Ahmad, E. Alpi, E. H. Bowler-Barnett, R. Britto, H. Bye-A-Jee, A. Cukura, P. Denny, T. Dogan, T. Ebenezzer, J. Fan, P. Garmiri, L. J. Da Costa Gonzales, E. Hattton-Ellis, A. Hussein, A. Ignatchenko, G. Insana, R. Ishtiaq, V. Joshi, D. Jyothi, S. Kandasamy, A. Lock, A. Luciani, M. Lugaric, J. Luo, Y. Lussi, A. MacDougall, F. Madeira, M. Mahmoudy, A. Mishra, K. Moulang, A. Nightingale, S. Pundir, G. Qi, S. Raj, P. Rapposo, D. L. Rice, R. Saidi, R. Santos, E. Speretta, J. Stephenson, P. Tootoo, E. Turner, N. Tyagi, P. Vasudev, K. Warner, X. Watkins, R. Zaru, H. Zellner, A. J. Bridge, L. Aimo, G. Argoud-Puy, A. H. Auchincloss, K. B. Axelsen, P. Bansal, D. Baratin, T. M. Batista Neto, M.-C. Blatter, J. T. Bolleman, E. Boutet, L. Breuza, B. C. Gil, C. Casals-Casas, K. C. Echioukh, E. Coudert, B. Cucho, E. De Castro, A. Estreicher, M. L. Famiglietti, M. Feuermann, E. Gasteiger, P. Gaudet, S. Gehant, V. Gerritsen, A. Gos, N. Gruaz, C. Hulo, N. Hyka-Nouspikel, F. Jungo, A. Kerhornou, P. Le Mercier, D. Lieberherr, P. Masson, A. Morgat, V. Muthukrishnan, S. Paesano, I. Pedruzzi, S. Pilboud, L. Pourcel, S. Poux, M. Pozzato, M. Pruess, N. Redaschi, C. Rivoire, C. J. A. Sigrist, K. Sonesson, S. Sundaram, C. H. Wu, C. N. Arighi, L. Arminski, C. Chen, Y. Chen, H. Huang, K. Laiho, P. McGarvey, D. A. Natale, K. Ross, C. R. Vinayaka, Q. Wang, Y. Wang, and J. Zhang, “UniProt: the Universal Protein Knowledgebase in 2023,” *Nucleic Acids Research*, vol. 51, no. D1, pp. D523–D531, Jan. 2023. [Online]. Available: <https://academic.oup.com/nar/article/51/D1/D523/6835362>
- [76] K. Reinert, T. H. Dadi, M. Ehrhardt, H. Hauswedell, S. Mehringer, R. Rahn, J. Kim, C. Pockrandt, J. Winkler, E. Siragusa, G. Urgese, and D. Weese, “The SeqAn C++ template library for efficient sequence analysis: A resource for programmers,” *Journal of Biotechnology*, vol. 261, pp. 157–168, Nov. 2017.
- [77] B. Schmidt, F. Kallenborn, A. Chacon, and C. Hundt, “Cudasw++ 4.0: ultra-fast gpu-based smith-waterman protein sequence database search,” *bioRxiv*, pp. 2023–10, 2023.
- [78] Xilinx, “Xilinx vitis libraries.” [Online]. Available: https://xilinx.github.io/Vitis_Libraries
- [79] W. J. Dally, Y. Turakhia, and S. Han, “Domain-specific hardware accelerators,” *Communications of the ACM*, vol. 63, no. 7, pp. 48–57, Jun. 2020. [Online]. Available: <https://dl.acm.org/doi/10.1145/3361682>
- [80] N. P. Jouppi, C. Young, N. Patil, D. Patterson, G. Agrawal, R. Bajwa, S. Bates, S. Bhatia, N. Boden, A. Borchers *et al.*, “In-datacenter performance analysis of a tensor processing unit,” in *Proceedings of the 44th annual international symposium on computer architecture*, 2017, pp. 1–12.
- [81] H. Genc, A. Haj-Ali, V. Iyer, A. Amid, H. Mao, J. Wright, C. Schmidt, J. Zhao, A. Ou, M. Banister *et al.*, “Gemmini: An agile systolic array generator enabling systematic evaluations of deep-learning architectures,” *arXiv preprint arXiv:1911.09925*, vol. 3, no. 25, pp. 15–17, 2019.
- [82] X. Wei, C. H. Yu, P. Zhang, Y. Chen, Y. Wang, H. Hu, Y. Liang, and J. Cong, “Automated systolic array architecture synthesis for high throughput cnn inference on fpgas,” in *Proceedings of the 54th Annual Design Automation Conference 2017*, 2017, pp. 1–6.
- [83] N. Noll, M. Molari, L. P. Shaw, and R. A. Neher, “Pangraph: scalable bacterial pan-genome graph construction,” *Microbial Genomics*, vol. 9, no. 6, p. 001034, 2023.
- [84] G. Hickey, D. Heller, J. Monlong, J. A. Sibbesen, J. Sirén, J. Eizenga, E. T. Dawson, E. Garrison, A. M. Novak, and B. Paten, “Genotyping structural variants in pangenome graphs using the vg toolkit,” *Genome biology*, vol. 21, pp. 1–17, 2020.
- [85] H. T. Kung and C. E. Leiserson, “Systolic arrays (for vlsi),” in *Sparse Matrix Proceedings 1978*, vol. 1. Society for industrial and applied mathematics Philadelphia, PA, USA, 1979, pp. 256–282.
- [86] R. P. Brent and H.-T. Kung, “Systolic vlsi arrays for polynomial gcd computation,” *IEEE Transactions on Computers*, vol. 100, no. 8, pp. 731–736, 1984.
- [87] W. M. Gentleman and H. Kung, “Matrix triangularization by systolic arrays,” in *Real-time signal processing IV*, vol. 298. SPIE, 1982, pp. 19–26.
- [88] J. Cong, J. Lau, G. Liu, S. Neuendorffer, P. Pan, K. Vissers, and Z. Zhang, “FPGA HLS Today: Successes, Challenges, and Opportunities,” *ACM Transactions on Reconfigurable Technology and Systems*, vol. 15, no. 4, pp. 51:1–51:42, Aug. 2022. [Online]. Available: <https://dl.acm.org/doi/10.1145/3530775>
- [89] K. Rupnow, Y. Liang, Y. Li, and D. Chen, “A study of high-level synthesis: Promises and challenges,” in *2011 9th IEEE International Conference on ASIC*, Oct. 2011, pp. 1102–1105.
- [90] F. Fahim, B. Hawks, C. Herwig, J. Hirschauer, S. Jindariani, N. Tran, L. P. Carloni, G. Di Guglielmo, P. Harris, J. Krupa, D. Rankin, M. B. Valentin, J. Hester, Y. Luo, J. Mamish, S. Orgreni-Memik, T. Aarrestad, H. Javed, V. Loncar, M. Pierini, A. A. Pol, S. Summers, J. Duarte, S. Hauck, S.-C. Hsu, J. Ngadiuba, M. Liu, D. Hoang, E. Kreinar, and Z. Wu, “hls4ml: An Open-Source Codesign Workflow to Empower Scientific Low-Power Machine Learning Devices,” Mar. 2021, arXiv:2103.05579 [physics]. [Online]. Available: <http://arxiv.org/abs/2103.05579>
- [91] M. Shahshahani, B. Khabbazan, M. Sabri, and D. Bhatia, “A Framework for Modeling, Optimizing, and Implementing DNNs on FPGA Using HLS,” in *2020 IEEE 14th Dallas Circuits and Systems Conference (DCAS)*, Dallas, TX, USA: IEEE, Nov. 2020, pp. 1–6.
- [92] A. Barenghi, M. Madaschi, N. Mainardi, and G. Pelosi, “OpenCL HLS Based Design of FPGA Accelerators for Cryptographic Primitives,” in *2018 International Conference on High Performance Computing & Simulation (HPCS)*. Orleans: IEEE, Jul. 2018, pp. 634–641.

- [93] E. Homsirikamol and K. G. George, "Toward a new HLS-based methodology for FPGA benchmarking of candidates in cryptographic competitions: The CAESAR contest case study," in *2017 International Conference on Field Programmable Technology (ICFPT)*. Melbourne, VIC: IEEE, Dec. 2017, pp. 120–127.
- [94] D. Castells-Rufas, S. Marco-Sola, J. C. Moure, Q. Aguado, and A. Espinosa, "Fpga acceleration of pre-alignment filters for short read mapping with hls," *IEEE Access*, vol. 10, pp. 22 079–22 100, 2022.
- [95] K. Liyanage, H. Gamaarachchi, R. Ragel, and S. Parameswaran, "Cross layer design using hw/sw co-design and hls to accelerate chaining in genomic analysis," *IEEE Transactions on Computer-Aided Design of Integrated Circuits and Systems*, vol. 42, no. 9, pp. 2924–2937, 2023.
- [96] P. Meng, M. Jacobsen, M. Kimura, V. Dergachev, T. Anantharaman, M. Requa, and R. Kastner, "Hardware accelerated novel optical de novo assembly for large-scale genomes," in *2014 24th International Conference on Field Programmable Logic and Applications (FPL)*, 2014, pp. 1–8.
- [97] K. Benkrid, Ying Liu, and A. Benkrid, "A Highly Parameterized and Efficient FPGA-Based Skeleton for Pairwise Biological Sequence Alignment," *IEEE Transactions on Very Large Scale Integration (VLSI) Systems*, vol. 17, no. 4, pp. 561–570, Apr. 2009. [Online]. Available: <http://ieeexplore.ieee.org/document/4773142/>